Citation: Rajanikanta Singh, M., 2022. Geochemistry of metabasites from the western Singhbhum Craton, eastern India: implications for subduction-zone tectonics and mantle-wedge metasomatism. Geologica Acta, 20.11, 1-15, I-III.
DOI: 10.1344/GeologicaActa2022.20.11

geologica acta

Geochemistry of metabasites from the western Singhbhum Craton, eastern India: implications for subduction-zone tectonics and mantle-wedge metasomatism

Mutum Rajanikanta Singh

Wadia Institute of Himalayan Geology
33 GMS Road, Dehradun-248001, Uttarakhand, India
E-mail: rajanimutum@gmail.com

ABSTRACT

The identification of new rock types in the volcano-sedimentary sequences of the Singhbhum Craton has attracted much attention in recent years. The present study deals on newly identified Nb-Enriched Basalts (NEB) from the Khandadharpahar-Kadakala-Thakuranipahar (KKT) section, western Singhbhum Craton, which is comparable in composition to basalts-basaltic andesites and calk-alkaline in character. These metabasites have a porphyritic texture with phenocrysts of pyroxene and plagioclase, as well as a groundmass that has metamorphosed to the greenschist facies. High Nb contents (7.5-22.8ppm) combined with high $(Nb/Th)_{PM}$ (0.28-0.59), $(Nb/La)_{PM}$ (0.40-0.69) and Nb/U (11.7-34.4) ratios, compared to arc basalts ($(Nb/Th)_{PM}$= 0.10-1.19; $(Nb/La)_{PM}$ 0.17-0.99, Nb/U<10), characterized them as NEB. Negative Nb, Zr, Hf and Ti anomalies, and Nb/Th vs La/Nb and Th/Nb vs. La/Sm relationships, collectively indicate typical arc volcanics. The available geochemical parameters suggest a genesis of KKT metabasites through i) slab melt migration from the downgoing oceanic crust, ii) low-degree melting of the garnet-bearing peridotite in the mantle wedge metasomatized by the slab melts, iii) slab melt - peridotite interaction triggering increasing Nb concentrations and iv) NEB generation in an arc-related environment. The discovery of KKT NEB sheds new information on Paleoproterozoic subduction-zone processes and crustal growth in the Singhbhum craton.

KEYWORDS | **Singhbhum Craton. Porphyritic texture. Nb-Enriched Basalts. Slab Melting. Mantle Wedge Metasomatism.**

INTRODUCTION

Mafic magmatic rocks developed on convergent plate margins provide critical clues to decipher mantle nature, tectonic processes and geodynamic evolution of crustal growth (Elliott *et al.*, 1997; Hawkesworth *et al.*, 1993; Hoang and Uto, 2006; Pearce and Peate, 1995; Perfit *et al.*, 1980; Spandler and Pirard, 2013). The subduction-related mafic volcanic rock associations, like calc-alkaline basalts, andesites, dacites and rhyolites, with minor occurrences of Ocean Island Basalts (OIB), boninites, picrites, adakites, High-Mg Andesites (HMA), high-Nb basalts (HNB) and Nb-Enriched Basalts (NEB), have been reported from various Archean-Proterozoic greenstone belts of the Superior Province (Canada), the Yangtze Craton (China) and the Singhbhum and Dharwar Cratons, India (Castillo, 2012; Han and Peng, 2020; Hollings and Kerrich, 2000; Hollings, 2002; Karsli *et al.*, 2021; Kerrich and Manikyamba, 2012; Khanna *et al.*, 2015; Liu *et al.*, 2014; Percival *et al.*, 2003; Polat and Kerrich, 2001; Ujike *et al.*, 2007; Wyman *et al.*, 2000). NEB are special mafic volcanic rocks formed in active

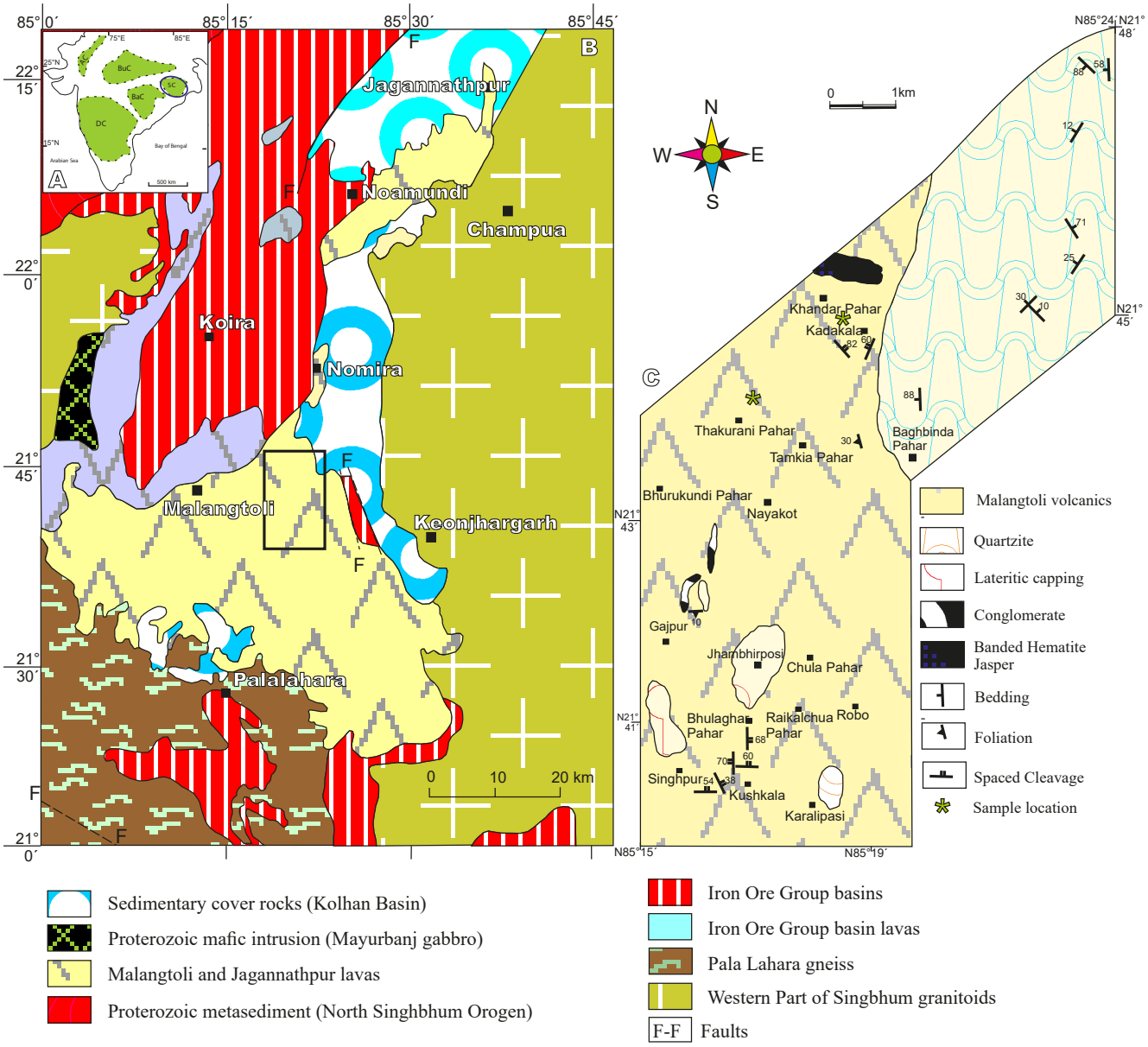

FIGURE 1. A) Inset map showing different cratons in southern peninsular India (map after Sharma, 2009; DC: Dharwar Craton, BaC: Bastar Craton, BuC: Bundelkhand Craton, SC: Singhbhum Craton, AC: Aravalli Craton), B) Simplified geological map of Singhbhum Craton (modified after Saha, 1994 and Misra, 2006) and C) local geological map of Malangtoli region with sample locations.

margins and have attracted much attention in recent years. They are characterized by high Nb contents (>7ppm in contrast to <2ppm in normal arc basalts), (Nb/La)PM< 0.5, high absolute abundances of HFSE, and low LILE/HFSE and HREE/LREE ratios (Azizi *et al.*, 2014; Hastie *et al.*, 2011; Mazhari, 2016). Partial melting of a mantle wedge metasomatized by adakitic melts is thought to be responsible for Nb enrichment in NEB (Aguillón-Robles *et al.*, 2001; Defant *et al.*, 1992; Petrone and Ferrari, 2008; Sajona *et al.*, 1996). Unlike OIB or shallow subduction of hot, young oceanic crust, where adakites are formed by melting of the subducted slab, NEB are generally linked with adakites. NEB, on the other hand, have different chemical compositions compared to adakitic melts, indicating that the source magmas did not come directly from the primitive mantle. Therefore, NEB are thought to be generated by metasomatized mantle melting along with flux from the heated oceanic lithosphere (Hastie *et al.*, 2011; Polat and Kerrich, 2001; Sajona *et al.*, 1993; Wang *et al.*, 2007).

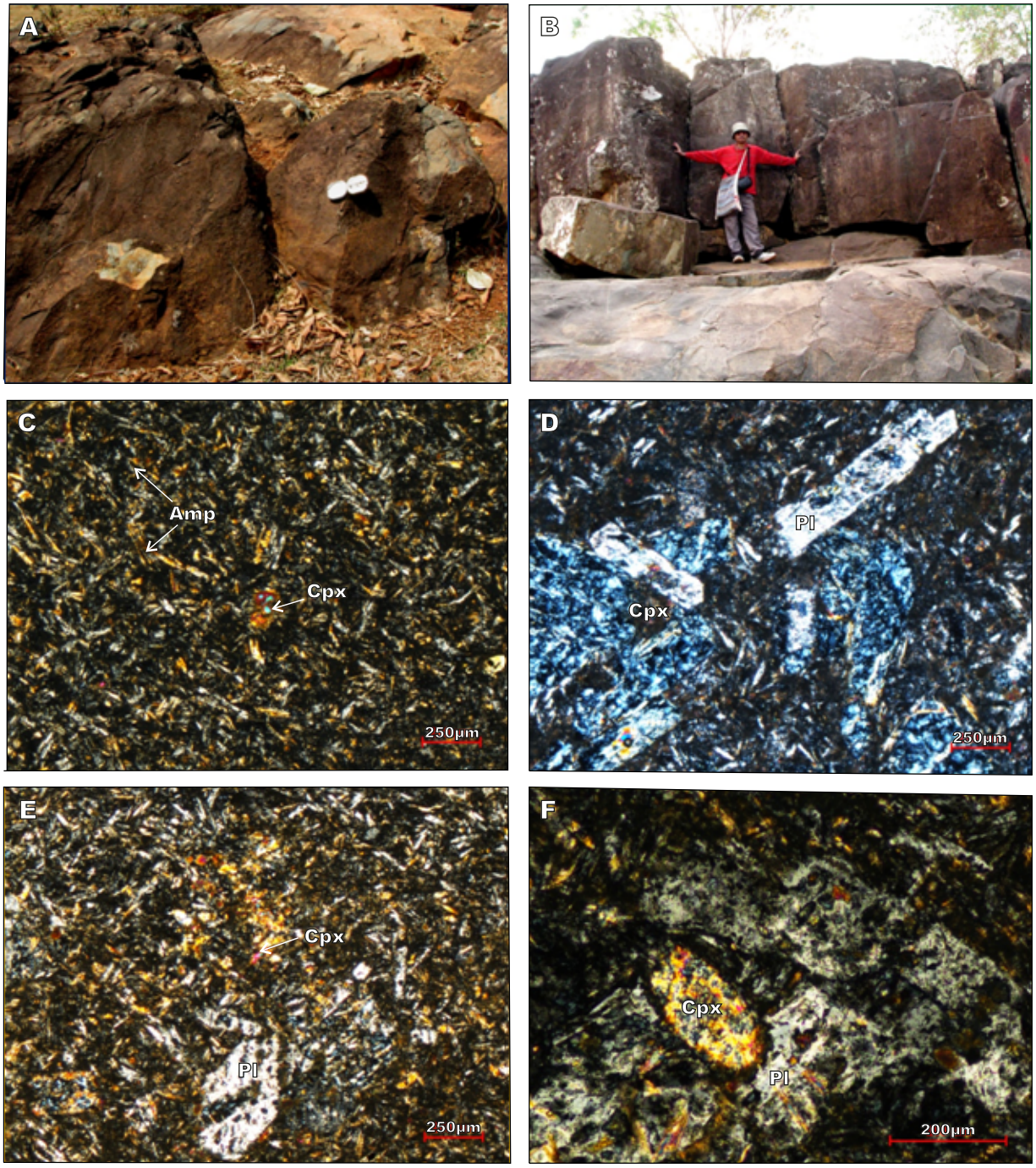

FIGURE 2. A, B) Field photographs of Khandadharpahar-Kadakala-Thakuranipahar (KKT) metabasites showing massive outcrops. C, D, E, F) Photomicrographs of plagioclase and pyroxene phenocrysts and amphiboles in the groundmass of metabasites, displaying intergranular, intersertal, and porphyritic texture.

Several previously unknown mafic magmatic rock types in the Singhbhum Craton (SC) have been discovered through geochemical studies over the last decade. In India, NEB have been reported from the Dharwar and SC (Kerrich and Manikyamba, 2012; Paul *et al.*, 2020; Singh *et al.*, 2017), and their geochemical systematics attest to the operation of Phanerozoic-type subduction-zone processes during the Neaorchean era. This paper discusses the magmatic and tectonic characteristics that control NEB genesis in ~2.2Ga old Malangtoli volcanic rocks from the western SC, as well as limitations on Proterozoic subduction-zone dynamics in eastern India.

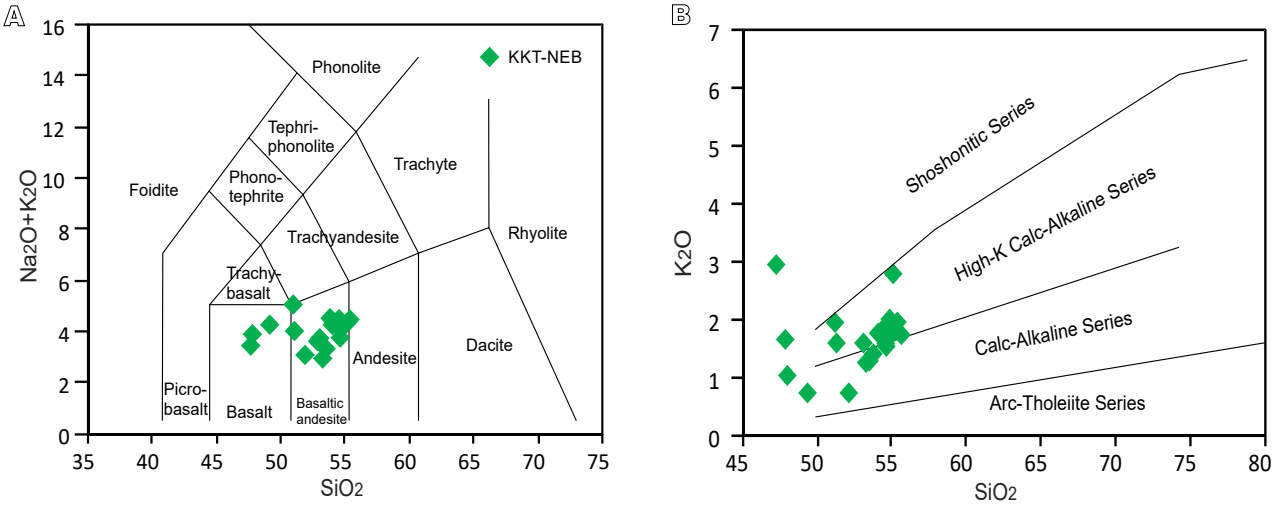

FIGURE 3. A) Total Alkali Silica (TAS) classification diagram (Le Bas *et al.*, 1986) and B) SiO_2 versus K_2O discrimination figures (Peccerillo and Taylor, 1976) showing the distribution of Khandadharpahar-Kadakala-Thakuranipahar (KKT) mafic rocks in the basalt-basaltic andesite and medium to high-K calc-alkaline field.

Geological settings

The SC is one of the oldest of the four major Archaean Cratons that make up the Indian Peninsula (Figure 1A; Dharwar, Aravalli-Bundelkhand, Bastar, and Singhbhum). Saha (1994) divided the SC into four principal litho-units namely i) Older Metamorphic Group (OMG) and Older Metamorphic Tonalite Gneiss (OMTG), ii) large granitic massifs of Singhbhum Granite (SBG), Bonai Granite (BG), Kaptipada (Nilgiri) Granite (KG), Mayurbhanj Granite (MBG) and Pallahara Gneiss (PG), iii) supracrustal rocks of several Iron Ore Basins and iv) belts of younger supracrustal rocks (Malangtoli Volcanics, the Jagannathpur Volcanics and the Ongarbira Volcanics, the dyke swarms of Newer Dolerite, and the intrusive bodies of ultramafics-gabbro-anorthosite suite).

Granitoids and associated enclaves make up the earliest components of SC, known as the "Singhbhum nucleus," which is bordered by volcano-sedimentary associations and supracrustal sequences (Bose, 2009; Pandey *et al.*, 2019; Saha, 1994; Sreenivas *et al.*, 2019; Weaver, 1990). The Singhbhum granite batholith (Misra, 2006; Saha, 1994) is a composite granitic pluton varying in age between 3.4 and 3.1Ga, which hosts enclaves of OMTG and OMG. Tonalite-trondhjemite-granodiorite gneisses of the OMTG represent the oldest suite of rocks with vestiges of Hadean zircon in the SC (Chaudhuri *et al.*, 2018). The SC has a long record of mafic magmatism, dating from the early Archaean to Proterozoic. However, the lack of adequate isotopic age data made it difficult to accurately reconstruct the history of spatial growth of the Craton in which mafic magmatism played a very significant role (Bose, 2009). The earliest phases of mafic magmatic activity in the SC are represented by i) mafic enclaves within the OMG (~3.3Ga), ii) ~3.1Ga mafic lavas of Iron-Ore Group (IOG) and iii) mafic-ultramafic rocks of Dalma-Dhanjori-Jagannathpur-Simplipal-Malangtoli volcanics, which are either younger or nearly contemporaneous with the Singhbhum Group of rocks (~2.2Ga; Adhikari *et al.*, 2021; Bose, 2000, 2009; Saha, 1994).

Over the borders of the western SC, various basalt-dominated volcanic or volcano-sedimentary successions emerged (Figure 1B). The stratigraphic status and age of these sequences are controversial due to the lack of geochronological data. Among them, the Malangtoli volcanic rocks are exposed to share a tectonic contact with the Banded Iron Formation (BIF) of IOG and cover an area of over 800km^2 to the west of Keonjhargarh town between Malangtoli (21˚45'N: 85˚15'E) in the north and Pala Lahara (21˚28'N: 85˚15'E) in the South (Figure 1B, C; Banerjee *et al.*, 2016; Bose, 2009; Ray *et al.*, 2006; Saha, 1994). Along the Southern boundary of Malangtoli lavas, the gently southwardly dipping quartzite-sandstone with pebble beds overlie the lavas on an unconformity. On the eastern side, the lavas are overlain by the Kolhan Group of sediments (Figure 1B). In general, the Malangtoli areas are predominantly metabasites with sporadic occurrences of quartzite, conglomerate, laterite and a lensoidal body of Banded Hematite Jasper (BHJ) (Figure 1C). The quartzite encountered in the field area is mainly of massive type though in some cases prominent bedding planes have been observed. Occasionally, small patches of conglomerate are found within the volcanic terrane, and a lensoidal body of BHJ is present in the Khandadhar Pahar area. In the Singhbhum Craton, NEB are recently reported from the Kushakala and Banspal areas of the Malangtoli (Singh *et*

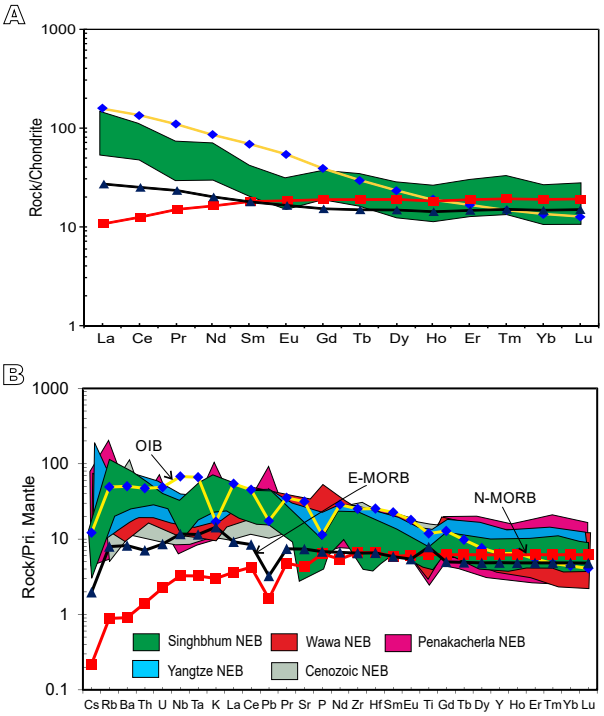

FIGURE 4. A) Chondrite-normalized rare-earth-element distributions and B) Primitive-Mantle-normalized trace-element spidergram for the studied metabasites. The normalization values for chondrite, primitive mantle, OIB (Ocean Island Basalt), E-MORB (Enriched Mid-Ocean Ridge Basalt) are from Sun and McDonough (1989). The trace-element fields of Khandadharpahar-Kadakala-Thakuranipahar (KKT) and Nb Enriched Basalts (NEB) along with their counterparts are from the Neoarchean Penakacherla greenstone belt (Dharwar Craton, India; Kerrich and Manikyamba, 2012), Wawa greenstone belt (Superior Province, Canada) and Cenozoic NEB (Panama, Northern Kamchatka, Philippines, Baja California (Defant *et al.*, 1992; Kepezhinskas *et al.*, 1996; Sajona *et al.*, 1996; Polat and Kerrich, 2001; Benoit *et al.*, 2002) exhibit consistent behaviors.

al., 2017) and Koira sectors of the western IOG basin (Paul *et al.*, 2020). Ray *et al.* (2006) studied the petrography and geochemistry of metavolcanic rocks from the restricted areas of Bayapandadar-Kanjipani in Malangtoli lavas and concluded that they are characterized by i) mostly basaltic andesites, ii) range in composition from tholeiitic to calc-alkaline in character, iii) derived from partial melting (20%) of the mantle which underwent subsequent pyroxene-hornblende-plagioclase fractionation, and iv) form at the transitional tectonic setting from ridge to Island Arc Tholeiite (IAT). Considering the lack of petrographic and geochemical data from the other parts of Malangtoli, in this study, metabasites of Khandadharpahar-Kadakala-Thakuranipahar (Figure 2A, B) sectors have been selected for petrological and geochemical studies. This study addresses the genesis of Khandadharpahar-Kadakala-Thakuranipahar (KKT) NEB through the interaction of slab melts and mantle-wedge metasomatism at a subduction zone that have contributed to the Paleoproterozoic subduction-zone processes and crustal growth in the Singhbhum Craton.

ANALYTICAL TECHNIQUES

Twenty-six fresh whole-rock samples were crushed and ground to ~200mesh using an agate mortar for elemental analyses at the National Geophysical Research Institute (NGRI), Hyderabad. Major oxides were determined by using pressed pellets on X-Ray Fluorescence (XRF) spectrometry (Phillips MAGIX PRO Model 2440) following the method of (Krishna *et al.*, 2007).

Trace element (including REE) concentrations were determined by Inductively Coupled Plasma Mass Spectrometry (ICP-MS; Perkin Elmer SCIEX ELAN DRC II). A closed digestion method was adopted in which a mixture of doubly distilled acids (HF+HNO_3+HCl, 5:3:2ml) was added to ca. 50mg rock powder in Savillex Vessels and kept on a hot plate at 150°C for three days. Following this, the entire mixture was evaporated to dryness. The decomposition procedure was repeated by adding 5ml of the above acid mixture for two days. When the sample was dry, 10ml of 1:1 $HNO_3$was added and heated at 150°C for 10-15min. Then 5ml Rh (1ppm concentration) was added as an internal standard. After cooling, the volume of the solution was made up to 250ml. Certified reference materials BHVO-1 and JB-2 were run as standards (Table I) to check the reproducibility. ^{103}Rh was used as an internal standard and external drift was corrected by repeated analyses of standards which were also used as calibration standards. Precision and reproducibility obtained for international reference materials are given in Table I that are found to be better than 2% Relative Standard Deviation (RSD) for the majority of the trace elements.

RESULTS

Petrography

Thin sections of mafic rocks are showing porphyritic texture consisting of pyroxenes and plagioclase as essential minerals with volcanic glass and opaque as accessory phases. Clinopyroxene and plagioclase occur as phenocrysts, while clinopyroxene, plagioclase, and volcanic glass make up the groundmass (Figure 2C, D, E, F). Plagioclase phenocrysts are saussuritized at some places and found in clusters within the groundmass showing intergranular texture (Figure 2D, F). Clinopyroxenes are altered to chlorite and at some places show alteration to fibrous amphibole, mainly actinolite and tremolite, suggesting greenschist-facies metamorphism. Opaques are iron oxides, mainly magnetite and chrome magnetite. Intergranular, intersertal, porphyritic, and variolitic igneous textures are all present in these rocks, indicating typical basaltic mineralogical assemblages.

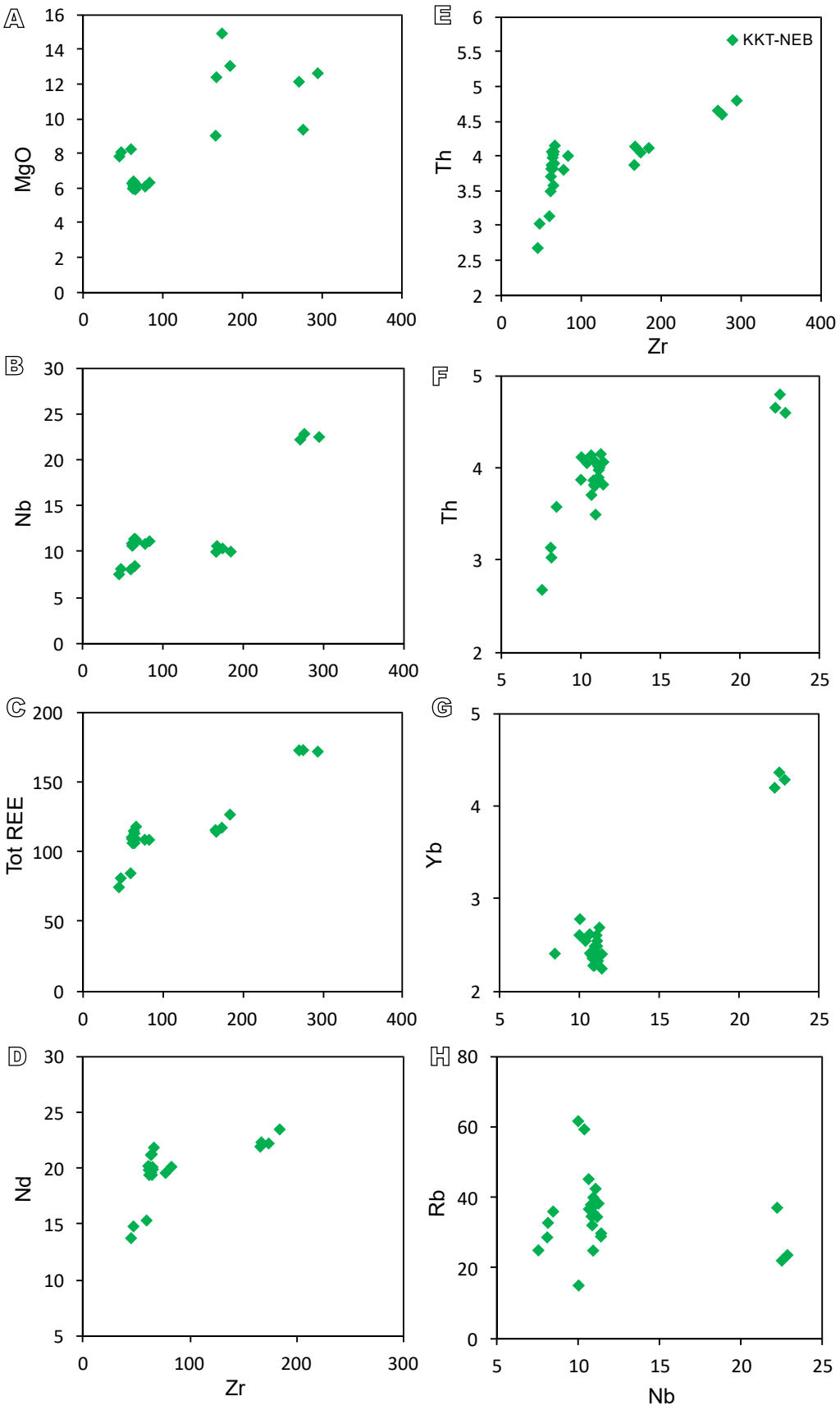

FIGURE 5. Zr versus selected MgO, REEs and HFSEs variation diagram showing good correlation and immobile features.

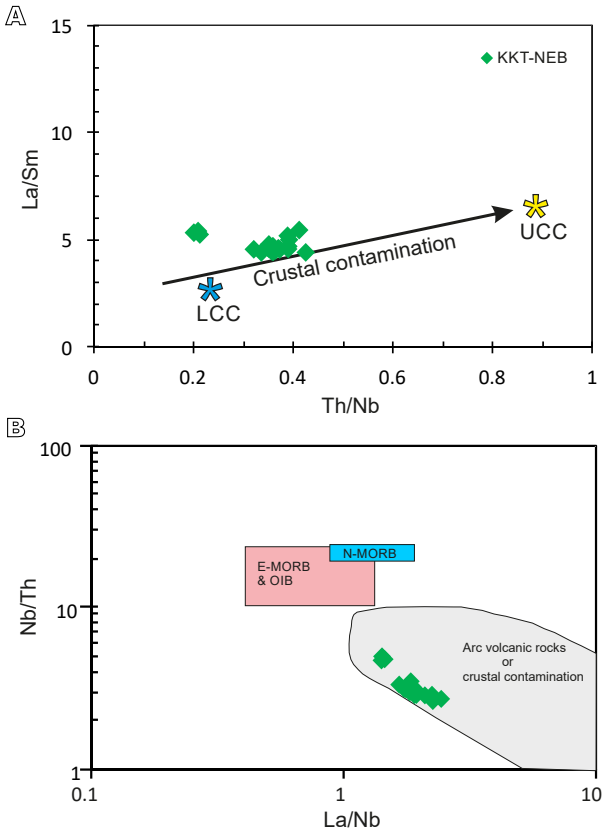

FIGURE 6. A) Th/Nb vs. La/Sm in which KKT metabasites are falling near LCC (Wang *et al.*, 2008). Data for LCC: lower continental crust and UCC: upper continental crust obtained from (Rudnick and Gao, 2003), B) Nb/Th vs La/Nb diagram showing typical arc volcanic signature.

Major oxides and trace elements

The studied basaltic rocks have silica contents between 47.27 to 55.65wt.% (average 53.18wt.%; Table II) and plot within the basalt and basaltic andesite fields (metabasites) in the total alkali silica diagram (Figure 3A). These are sodic (Na_2O/K_2O= 1.16-5.01, except for one sample) and fall in the medium- to high-K calc-alkaline field (Figure 3B). The MgO content of the metavolcanic rocks ranges from 5.9 to 14.9wt.% with variability in their alkali content (1.8-7.0wt.%). These metabasites have moderate TiO_2 (0.84-1.14wt.%), Al_2O_3 (10.5 - 13.5wt.%), K_2O (1.2-2.0wt.%) and Na_2O (1.7-2.9wt.%) contents, with uniformly low P_2O_5 (0.09-0.13wt.%) and MnO (0.14-0.18wt.%). Fe_2O_3 ranges from 11.2 to 15.3wt.%. Though these samples show moderate to high MgO, their ferromagnesian trace-element contents are very low. Their Rb, Sr and Zr contents are 25-62ppm, 68-321ppm and 45-294ppm, respectively.

These metabasites have Nb concentrations ranging from 7.5 to 22.8ppm (Table II). The high Nb content combined with high $(Nb/Th)_{PM}$ (0.28-0.59), $(Nb/La)_{PM}$ (0.40-0.69) and Nb/U (11.7-34.4) ratios, compared with arc basalts ($(Nb/Th)_{PM}$= 0.10-1.19; $(Nb/La)_{PM}$ 0.17-0.99, Nb/U<10), characterize them as Nb-enriched basalts. On a chondrite-normalized REE diagram (Figure 4A), the samples show LREE enrichment and subhorizontal HREE patterns (La/Yb_{CN}= 5.25-6.35; Gd/Yb_{CN}= 1.39-1.98), with negative Eu anomalies (Eu/Eu^*= 0.55-0.91). On the primitive-mantle-normalized trace-element diagram (Figure 4B), these rocks exhibit negative Nb, Zr, Hf and Ti anomalies. However, the REE and multi-element patterns deviate from the usual OIB, Enriched mid-ocean ridge basalts (E-MORB) and Normal mid-ocean ridge basalts (N-MORB) patterns (Figure 4B). These characteristics are analogous to those of Precambrian and Phanerozoic NEB (Aguillon-Robles *et al.*, 2001; Castillo, 2008; Hollings, 2002; Liu *et al.*, 2017, 2018; Sajona *et al.*, 1996; Wang *et al.*, 2013).

DISCUSSION

Effect of alteration, element mobility and crustal contamination

Understanding the petrogenesis of basaltic rocks requires a thorough examination of the trace elements that remain immobile during hydrothermal activity and metamorphism (Lesher *et al.*, 2001; Song *et al.*, 2006). The rocks analysed in this study did not undergo any significant secondary alteration as inferred from their lower values of LOI (0.06-2.20wt.%) and lack of carbonization or silicification. Most samples, however, show a small range of Ce/Ce^* ratios (1.13-1.20), indicating that LREE mobility is limited (Polat *et al.*, 2002). HFSEs and REEs are trapped in the structures of secondary minerals because of their high valencies, electronegativity, small radii and strong chemical bonds when their primary host minerals are destroyed during alteration processes. These elements maintain constant ratios and good linear correlations, which attest to their immobility during hydrothermal changes and metamorphism (Said and Kerrich, 2009; Song *et al.*, 2006). HFSEs and REEs display a good correlation with Zr and Nb on variation diagrams (Figure 5), indicating that these elements have not been significantly mobilized during greenschist facies metamorphism and hydrothermal alteration.

NEB do not correspond to primordial magmas, as they show varying degrees of crystal fractionation and are contaminated by tholeiitic mantle or crustal components (Castillo, 2008). Primary mantle-derived melts tend to have high Cr (>400ppm) and Ni (>1000ppm) contents (Litvak and Poma, 2010). The low Cr (23-96ppm) and Ni (23-62ppm) contents and their negative correlation of KKT NEB indicate olivine or clinopyroxene fractionation (Xu *et al.*, 2019). The lack of significant Eu anomalies (Eu/Eu^*= 0.55-0.91) suggests little or no plagioclase fractionation. Negative Nb-Ta anomalies and negative to positive Zr-Hf

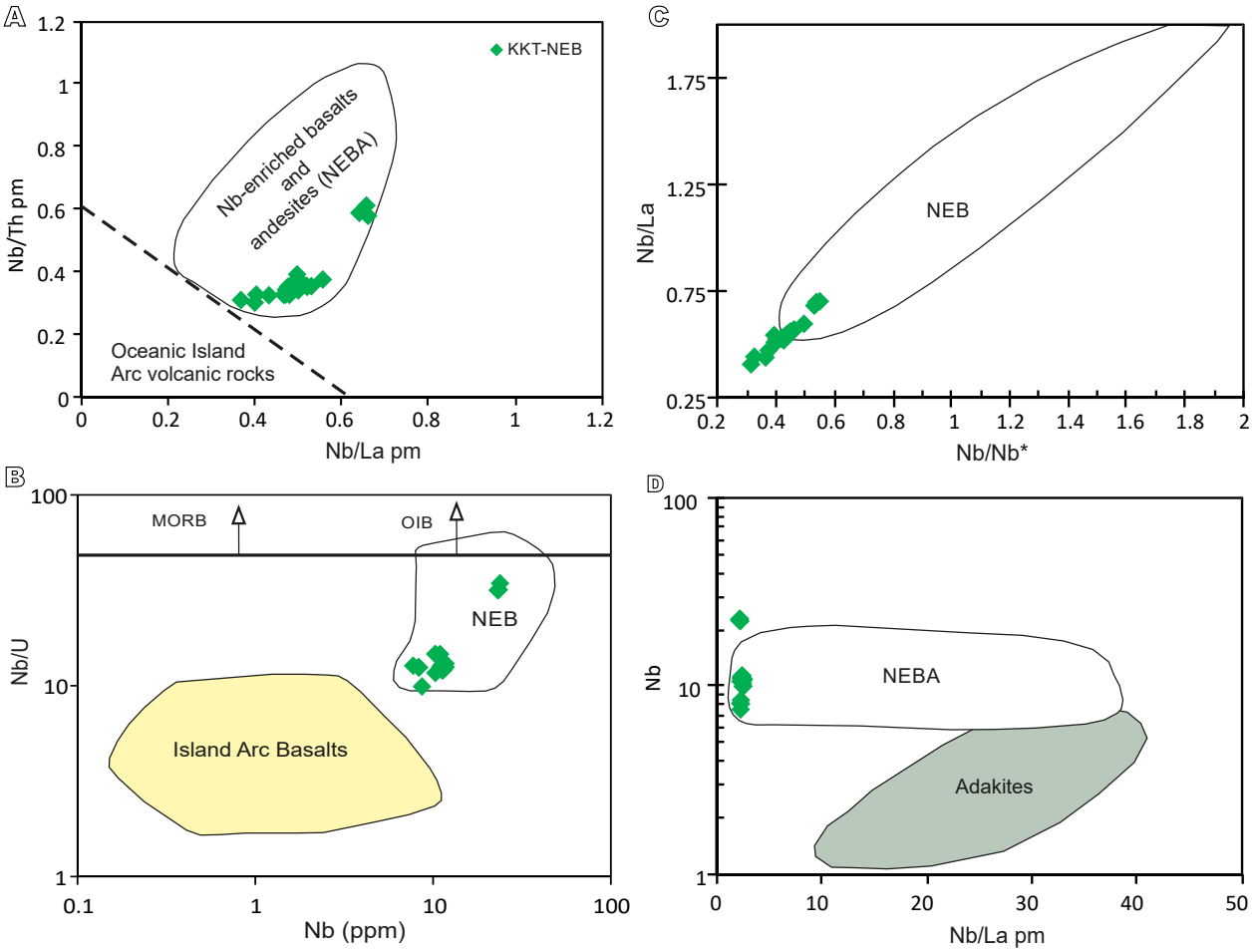

FIGURE 7. A) Nb/La_{PM} versus Nb/Th_{PM} diagram (Sajona *et al.*, 1996; Kepezhinskas *et al.*, 1997; Aguillon-Robles *et al.*, 2001); B) Nb/U versus Nb diagram (Kepezhinskas *et al.*, 1996); C) Nb/Nb* vs Nb/La diagram (Petrone *et al.*, 2006); D) Nb vs La/Yb_{PM} diagram (Polat and Kerrich, 2001), in which the KKT NEB are plotting in the field of the Phanerozoic NEB.

anomalies (Figure 4B), Nb/Th vs. La/Nb, and Th/Nb vs. La/Sm relationships (Figure 6) clearly indicate a typical arc volcanic signature with limited crustal contamination of the studied samples (Rudnick and Gao, 2003; Wang *et al.*, 2008). Such contamination may not have strongly influenced other immobile elements.

Petrogenesis: mantle-wedge metasomatism

NEB have some geochemical similarities to Island Arc Basalts (IABs), but they have higher Nb and other HFSE contents, as well as a high Nb/La_{PM} ratio (>0.5). In Figures 7A, B, C, D, KKT NEB plot above the diagonal line distinguishing the NEB field from the arc basalts and andesites (Polat and Kerrich, 2001), similarly to the Nb-enriched basalts described by Hollings and Kerrich (2000), Martin *et al.* (2005) and Sajona *et al.* (1996). Compared to OIBs (Nb= 48ppm; Sun and Mcdonough, 1989), NEB have lower Nb concentrations (KKT NEB≤ 22.8; Sajona *et al.*, 1993; Wyman *et al.*, 2000; Hollings, 2002), and hence lower Nb/U ratios (Kepezhinskas *et al.*, 1996; Sajona *et al.*, 1993, 1996). Several hypotheses for explaining the geochemical properties of Nb-enriched mafic rocks have been presented based on previous research, including i) partial melting of the enriched mantle with a component of OIB (Castillo, 2008; Petrone and Ferrari, 2008; Sorbadere *et al.*, 2013), ii) ascending magma assimilating crustal/sediment material, and iii) above a subduction zone, melting of a hybridized mantle wedge (Aguillon-Robles *et al.*, 2001; Polat and Kerrich, 2001; Sajona *et al.*, 1993; Smithies *et al.*, 2005; Wang *et al.*, 2007, 2008; Zhang *et al.*, 2005). The lower Nb/U (<31) and Ce/Pb (<8) ratios of KKT NEB do not support their generation by melting of OIB/enriched mantle source. Positive Nb anomalies are found in magmas produced from OIB sources. The studied samples with significant Nb enrichment, on the other hand, display negative Nb anomalies (Figure 4B), ruling out the possibility of an OIB component in the mantle source.

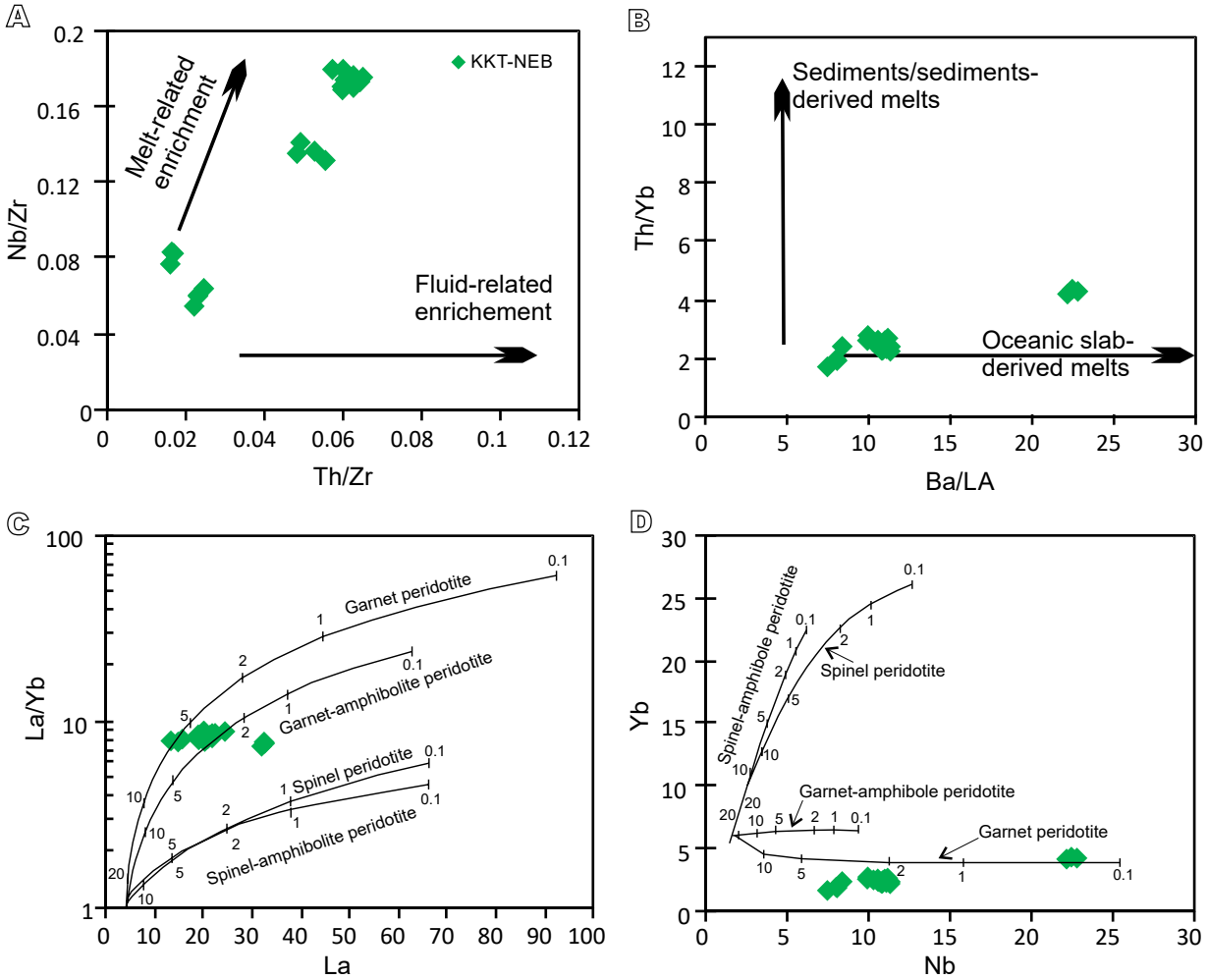

FIGURE 8. Plots of A) Nb/Zr versus Th/Zr (Kepezhinskas *et al.*, 1997) and B) Th/Yb versus Ba/La (Furman and Graham, 1999). The diagrams of C) La/Yb versus La and D) Yb versus Nb, include simple geochemical modeling for the KKT NEB. The non-modal batch melting curves are given for garnet peridotite ($Olivine_{0.6}Orthopyroxene_{0.2}Clinopyroxene_{0.1}Garnet_{0.1}$: Johnson, 1998), garnet amphibole peridotite ($Ol_{0.55}Opx_{0.22}Cpx_{0.15}Grt_{0.05}Amp_{0.01}$: Barry *et al.*, 2003) and spinel peridotite ($Ol_{0.53}Opx_{0.27}Cpx_{0.17}Sp_{0.03}$: Johnson, 1998). Normative weight fractions of mineral i in the partial melts are $Ol_{0.1}Opx_{0.18}Cpx_{0.3}Grt_{0.42}$ (Johnson, 1998), $Ol_{0.05}Opx_{0.05}Cpx_{0.3}Grt_{0.2}$ $Amp_{0.1}$ (Barry *et al.*, 2003) and $Ol_{-0.4}Opx_{0.3}Cpx_{0.9}Sp_{0.2}$ (Kelemen *et al.*, 1993). Mineral-melt distribution coefficients utilized for the geochemical modelings are after Green (1994) for Nb and Mckenzie and O'Nions (1991) for REE. Starting compositions are basalt from the enriched mantle (La = 0.74 ppm, Yb = 0.67 ppm, and Nb=0.5 ppm; Wang *et al.*, 2004).

The Nb enrichment with lower LILE/HFSE ratios of the studied NEB rules out crustal/sediment assimilation during magma ascent which otherwise would have resulted in extremely elevated LILE concentrations. Though NEB is a specific rock type found in few cratons, the available data suggest that these are characteristic rock types generated at convergent margins where slab melts play a vital role in the metasomatism of the mantle wedge. Mantle sources modified by slab melts are likely to have lower Th/Zr and Rb/Y than those modified by fluids (Kepezhinskas *et al.*, 1997; Wang *et al.*, 2007). Their Th/Zr ratios are narrowly changeable, whereas their Nb/Zr ratios are extensively variable (Figure 8A), implying that the enrichment is most likely due to subduction-related melt rather than fluids. The Th/Yb vs. Ba/La diagrams further indicates that a melt-related enrichment (oceanic-slab-generated melt) was most likely a metasomatic agent (Figure 8B).

On La/Yb ratio vs. La and Yb vs Nb diagrams (Figure 8C, D; Karsli *et al.*, 2021), the studied samples plot between melting curves of the garnet-bearing peridotite and garnet-amphibole-bearing peridotite with low melting degrees (<3%). According to the modeling, the KKT NEB could originate from garnet and amphibole-bearing mantle lithologies metasomatized by slab melts. Sajona *et al.* (1993, 1996) and Kepezhinskas *et al.* (1996) propose that melting of subducted oceanic slabs occurs at temperatures above 700°C. and at depths of 75 to 85 kilometers. Slab melts have more HFSE than hydrous fluids, and they ascend to percolate into the mantle wedge, causing hybridization and metasomatism (Thirlwall *et*

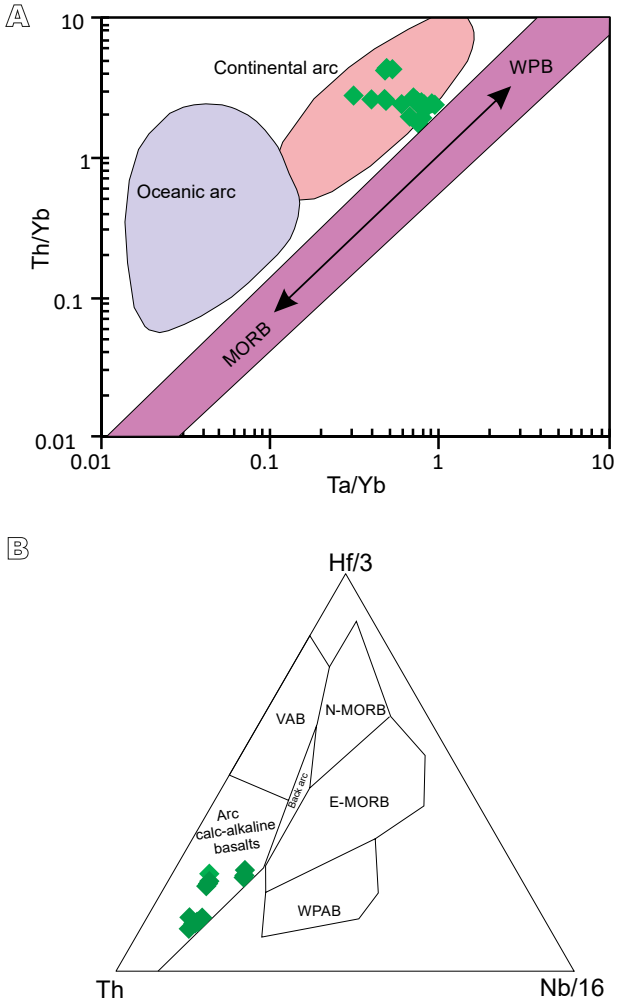

FIGURE 9. Tectonic discrimination plots of A) Th/Yb versus Ta/Yb (Pearce, 1982) and B) Hf/3-Th-Nb/16 (Wood, 1980) for KKT metabasites.

al., 1994). The reaction between slab melts and mantle-wedge peridotite (Rapp, *et al.*, 1999) breaks down olivine, orthopyroxene, clinopyroxene and spinel forming Nb- and Ti-enriched pargasitic amphibole, garnet, phlogopite, Na-rich clinopyroxene and Fe-rich orthopyroxene (Tiepolo *et al.*, 2000). These metasomatic minerals trap HFSE (Nb, Ti, Ta) and decomposition of these phases in the convecting mantle peridotite trigger partial melting at depths above the zone of slab melting, generating NEB. The petrography, trace-element and rare-earth.element compositions of KKT NEB suggest partial melting of a mantle with Nb-rich phases (amphibole, ilmenite). As a result, the origin of KKT NEB is interpreted as caused by i) slab melt migration from the downgoing oceanic crust, ii) low-degree melting of the garnet-bearing peridotite in the mantle wedge metasomatized by the slab melts, iii) slab melt - peridotite interaction increasing the Nb concentration and iv) NEB generation in an arc-related environment. Furthermore, the trace-element signatures of NEB (Figure 4B; 7) from Archaean (Neoarchean Penakacherla greenstone belt, Wawa greenstone belt, etc.) and Cenozoic (Panama, Northern Kamchatka, Philippines, Baja California) occurrences around the world show consistent behavior with the KKT NEB, suggesting a common origin.

TECTONIC IMPLICATIONS

The geochemical characteristics of modern volcanic rocks generated at various tectonic settings are rather similar in their LILE, HFSE and REE signatures (McCulloch and Gamble, 1991; Pearce and Parkinson, 1993; Pearce and Peate, 1995; Polat and Kerrich, 2001; Pearce, 2008). This observation is evident from many Archean and Proterozoic volcanic sequences that erupted through mantle-plume and subduction-zone processes (Han and Peng, 2020; Khanna *et al.*, 2015; Liao *et al.*, 2018; Manikyamba *et al.*, 2005; Polat and Kerrich 2006). Based on the geochemical fingerprints preserved in various litho-units belonging to varied ages by earlier workers (Polat and Kerrich, 2001), it has been advocated that a certain group of elements behaves coherently during a particular petrogenetic process throughout the Earth's history. The SC in eastern India shows excellent preservation of volcano-sedimentary sequences spanning the Paleo-Mesoarchean to Proterozoic periods, indicating a range of geodynamic events. However, understanding the petrogenesis and geodynamic context of these mafic volcanic litho-units requires geochemical characterization in terms of LILE, HFSE and REE. Following the identification of a wide spectrum of volcanic rocks from the Phanerozoic subduction zones, the greenstone belts of various cratons present on different parts of the globe have been revisited, leading to the identification of such rock types from many greenstone belts of India, Superior Province, Pilbara Craton and Greenland, thereby endorsing a Phanerozoic-type of plate tectonic processes during the Archean and Proterozoic. Previous workers suggest that subduction zones formed in arc regions (Aguillóne-Robles *et al.*, 2001; Avdeiko and BergaleKuvikas, 2015; Chen *et al.*, 2016; Liu *et al.*, 2014; Petrone and Ferrari, 2008; Petrone *et al.*, 2006; Sajona *et al.*, 1993, 1996; Shen *et al.*, 2014; Zhang *et al.*, 2016), the back-arc basin (Hollings, 2002; Sorbadere *et al.*, 2013; Wang *et al.*, 2013; Zhang *et al.*, 2012), post-collisional extension settings, and continental rifts are all considered to be a tectonic setting of NEB (Xia *et al.*, 2009). Based on Ce and Yb relationship, Hawkesworth *et al.* (1993) have distinguished a low Ce-Yb trend for interoceanic arcs such as South Sandwich, the Marianas and the Tonga Kermadec arc, and a high Ce-Yb trend for continental arcs such as the Andes and the Aeolian Islands. The KKT NEB are exhibiting a high Ce-Yb trend consistent with the signatures of continental arcs (Figure not shown). They also show similar behavior on the Th/Yb vs. Ta/Yb (Pearce, 1982) and

Th-Nb/16-Hf-3 tectonic discrimination diagrams (Figure 9), suggesting a subduction-related arc setting for the studied rocks. Such characteristics are almost identical to Nb-enriched basalts of the Philippines and Baja California (Aguillón-Robles *et al.*, 2001; Sajona *et al.*, 1996).

The presence of NEB in and around ~2.25Ga Malangtoli and ~3.1Ga Koira-Jamda (Iron Ore Group), have evidenced that considerable continental growth occurred during the Archaean and Proterozoic time span. One of the primary crustal growth mechanisms in the western SC was interval generations of slab melt from hot (and/or young) oceanic crustal subduction and mantle wedge metasomatism.

CONCLUSIONS

i) Khandadharpahar-kadakala-Thakuranipahar areas of Malangtoli preserve a rare occurrence of Nb-Enriched Basalts (NEB) in the western Singhbhum Craton (SC) which is geochemically similar to Archean and Phanerozoic NEB of the world.

ii) These NEB are medium- to high-K calc-alkaline with MgO ranging from 5.9 to 14.9wt.%, exhibiting variation in their alkali content (1.8-7.0wt.%) and low ferromagnesian trace-element contents. The higher Nb content (7.5-22.8ppm) of these metabasites combined with high $(Nb/Th)_{PM}$ (0.28-0.59), $(Nb/La)_{PM}$ (0.40-0.69) and Nb/U (11.7-34.4) ratios, compared with arc basalts ($(Nb/Th)_{PM}$= 0.10-1.19; $(Nb/La)_{PM}$= 0.17-0.99, Nb/U<10), characterize them as NEB.

iii) The KKT NEB are resembling the NEB of the Wawa greenstone belt (Superior Province), the Penakacherla greenstone belt of Dharwar Craton, and the Pliocene-Pleistocene Zamboanga Peninsula (western Mindanao). Most of the La/Nb ratios of KKT NEB are <2 which is within the range of NEB from the Pliocene-Pleistocene Zamboanga Peninsula and the Triassic NEB from the Qiangtang terrane (Central Tibet).

iv) The available geochemical characteristics support KKT NEB generation through partial melting of mantle-wedge peridotite with metasomatism of subduction-derived melts, resembling NEB generated in arc-related tectonic settings.

ACKNOWLEDGMENTS

The author is grateful to Dr. Kalachand Sain, Director, Wadia Institute of Himalayan Geology (WIHG) for his kind permission to publish this work. The motivation for this study comes from Dr. C Manikyamba (Ph.D. supervisor), Emeritus Scientist, CSIR-NGRI and Dr. Sohini Ganguly, Goa University. In addition, he would like to thank Prof. J. Ray for his assistance during the fieldwork. The constructive comments from the anonymous reviewers are greatly appreciated. This is WIHG's contribution no. 0180.

REFERENCES

Adhikari, A., Nandi, A., Mukherjee, S., Vadlamani, R., 2021. Petrogenesis of Neoarchean (2.80-2.75 Ga) Jagannathpur volcanics and the Ghatgaon and Keshargaria dyke swarms, Singhbhum craton, eastern India: Geochemical, Sr-Nd isotopic and Sm-Nd geochronologic constraints for interaction of enriched-DMM derived magma with metasomatised subcontinental lithospheric mantle. Lithos, 400-401, 106373.

Aguillon-Robles, A., Calmus, T., Benoit, M., Bellon, H., Maury, R.C., Cotten, J., Bourgois, J., Michaud, F., 2001. Late Miocene adakites and Nb-enriched basalts from Vizcaino Peninsula, Mexico: indicators of East Pacific Rise subduction below southern Baja California? Geology, 29(6), 531-534.

Avdeiko, G.P., Bergale Kuvikas, O.V., 2015. The geodynamic conditions for the generation of adakites and Nberich basalts (NEAB) in Kamchatka. Journal of Volcanology and Seismology, 9, 295-306.

Azizi, H., Asharana, Y., Tsuboi, M., 2014. Quaternary high-Nb basalts: existence of young oceanic crust under the Sanandaj-Sirjan Zone, NW Iran. International Geology Review, 56(2), 167-186.

Banerjee, M., Ray, J., Nandy, S., Manikyamba, C., Madhuparna, P., Chakraborthy, D., Eslami, A., 2016. Experimental studies to constrain parental magma of Malangtoli volcanics from Singhbhum craton of eastern Indian shield. Journal of Geological Society of India, 88, 245-255.

Barry, T.L., Saunders, A.D., Kempton, P.D., Windley, B.F., Pringle, M.S., Dorjnamjaa, D., Saandar, S., 2003. Petrogenesis of Cenozoic basalts from Mongolia: evidence for the role of asthenospheric versus metasomatized lithospheric mantle sources. Journal of Petrology, 44, 55-91.

Benoit, M., Aguillón-Robles, A., Calmus, T., Maury, R., Bellon, H., Cotton, J., Bourgois, J., Michard, F., 2002. Geochemical diversity of Late Miocene volcanism in southern Baja California, Mexico: implication of mantle and crustal sources during the opening of an asthenospheric window. The Journal of Geology, 110, 627-648.

Bose, M.K., 2000. Mafic - ultramafic magmatism in the eastern Indian craton - A review. Geological Survey of India, 55 (Special Publication), 227-258.

Bose, M.K., 2009. Precambrian mafic magmatism in the Singhbhum Craton, eastern India. Journal of Geological Society of India, 73, 13-35.

Castillo, P.R., 2008. Origin of the adakite-high-Nb basalt association and its implications for post subduction magmatism in Baja California, Mexico. Geological Society of America Bulletin, 120, 451-462.

Castillo, P.R., 2012. Adakite petrogenesis. Lithos, 134-135, 304-316.

Chaudhuri, T., Wan, Y., Mazumder, R., Ma, M., Liu, D., 2018. Evidence of enriched, Hadean mantle reservoir from 4.2-4.0 Ga zircon xenocrysts from Paleoarchean TTGs of the Singhbhum Craton, Eastern India. Scientific Reports, 8(7069), 1-12.

Chen, S.S., Shi, R.D., Yi, G.D., Zou, H.B., 2016. Middle Triassic volcanic rocks in the Northern Qiangtang (Central Tibet): geochronology, petrogenesis, and tectonic implications. Tectonophysics, 666, 90-102.

Defant, M.J., Jackson, T.E., Drummond, M.S., 1992. The geochemistry of young volcanism throughout western Panama and southeastern Costa Rica: An overview. London, Journal of the Geological Society, 149, 569-579.

Elliott, T., Plank, T., Zindler, A., White, W., Bourdon, B., 1997. Element transport from slab to volcanic front at the Mariana arc. Journal of Geophysical Research, Solid Earth, 102(B7), 14991-15019.

Furman, T., Graham, D., 1999. Erosion of lithospheric mantle beneath the East African Rift system: geochemical evidence from the Kivu volcanic province. Lithos, 48, 237-262.

Green, T.H., 1994. Experimental studies of trace-element partitioning applicable to igneous petrogenesis—Sedona 16 years later. Chemical Geology, 117, 1-36.

Han, Q., Peng, S., 2020. Paleoproterozoic subduction within the Yangtze Craton: Constraints from Nb-enriched mafic dikes in the Kongling complex. Precambrian Research, 340, 105634.

Hastie, A.R., Mitchell, S.F., Kerr, A.C., Minifie, M.J., Millar, I.L., 2011. Geochemistry of rare high-Nb basalt lavas: are they derived from a mantle wedge metasomatised by slab melts? Geochimica et Cosmochimica Acta, 75(17), 5049-5072.

Hawkesworth, C.J., Gallagher, K., Hergt, J.M., McDermott, F., 1993. Mantle and slab contributions in arc magmas. Annual Review of Earth and Planetary Sciences, 21(1), 175-204.

Hoang, N., Uto, K., 2006. Geochemistry of Cenozoic basalts in the Fukuoka district (northern Kyushu, Japan): implications for asthenosphere and lithospheric mantle interaction. Chemical Geology, 198, 249-268.

Hollings, P., Kerrich, R., 2000. An Archean arc basalt-Nb-enriched basalt-adakite association: the 2.7 Ga Confederation assemblage of the Birch-Uchi greenstone belt, Superior Province. Contribution to Mineralogy and Petrology, 139(2), 208-226.

Hollings, P., 2002. Archean Nb-enriched basalts in the northern Superior Province. Lithos, 64(1), 1-14.

Johnson, K.T.M., 1998. Experimental determination of partition coefficients for rare earth and high-field-strength elements between clinopyroxene, garnet, and basaltic melt at high pressures. Contribution to Mineralogy and Petrology, 133, 60-68.

Karsli, O., Ilhan, M., Kandemir, R., Dokuz, A., Aydin, F., Uysal, I., Duygu, L., 2021. Nature of the Early Cretaceous lamprophyre and high-Nb basaltic dykes, NE Turkey: Constraints on their linkage to subduction initiation of Neotethyan oceanic lithosphere. Lithos, 380, 105884.

Kelemen, P.B., Shimazu, N., Dunn, T., 1993. Relative depletion of niobium in some arc magmas and the continental crust: partitioning of K, Nb, La and Ce during melt/ rock reaction in the upper mantle. Earth and Planetary Science Letters, 120, 111-134.

Kepezhinskas, P.K., Defant, M.J., Drummond, M.S., 1996. Progressive enrichment of island arc mantle by melt-peridotite interaction inferred from Kamchatka xenoliths. Geochimica et Cosmochimica Acta, 60, 1217-1229.

Kepezhinskas, P., McDermott, F., Defant, M.J., Hochstaedter, A., Drummond, M.S., 1997. Trace element and Sr-Nd-Pb isotopic constraints on a three component model of Kamchatka Arc petrogenesis. Geochimica et Cosmochimica Acta, 61(3), 577-600.

Kerrich, R., Manikyamba, C., 2012. Contemporaneous eruption of Nb-enriched basalts-Kadakites- Na-adakites from the 2.7 Ga Penakacherla terrane: implications for subduction zone processes and crustal growth in the eastern Dharwar craton, India. Canadian Journal of Earth Sciences, 49(4), 615-636.

Khanna, T.C., Sai, V.V.S., Bizimis, M., Krishna, A.K., 2015. Petrogenesis of basalt-high-Mg andesite-adakite in the Neoarchean Veligallu greenstone terrane: Geochemical evidence for a rifted back-arc crust in the eastern Dharwar craton, India. Precambrian Research, 258, 260-277.

Krishna, A.K., Murthy, N.N., Govil, P.K., 2007. Multielement Analysis of Soils by Wavelength-Dispersive X-ray Fluorescence Spectrometry. Atomic spectrometry, 28(6), 202-214.

Le Bas, M.J., Maitre, R.W., Streckeisen, A., Zanettin, B., 1986. A chemical classification of volcanic rocks based on the total alkali and silica diagram. Journal of Petrology, 27, 45-750.

Lesher, C.M., Burnham, O.M., Keays, R.R., Barnes, S.J., Hulbert, L., 2001. Trace-element geochemistry and petrogenesis of barren and ore associated komatiites. Canadian Mineralogist, 39, 673-696.

Liao, F-X., Chen, N-S., Santosh, M., Wang, Q-Y., Gong, S-L., He, C., Mustafa, H.A., 2018. Paleoproterozoic Nbeenriched meta-gabbros in the Quanji Massif, NW China: Implications for assembly of the Columbia supercontinent. Geosciences Frontiers, 9, 577-590.

Litvak, V.D., Poma, S., 2010. Geochemistry of mafic Paleocene volcanic rocks in the Valle del Cura region: Implications for the petrogenesis of primary mantle-derived melts over the Pampean flat-slab. Journal of South American Earth Sciences, 29(3), 705-716.

Liu, C.H., Zhao, G.C., Liu, F.L., Shi, J.R., 2014. 2.2 Ga magnesian andesites, Nb-enriched basalt-andesites, and adakitic rocks in the Luliang Complex: evidence for early Paleoproterozoic subduction in the North China Craton. Lithos, 208, 104-117.

Liu, H., Wang, Y., Cawood, P.A., Guo, X., 2017. Episodic slab rollback and back-arc extension in the Yunnan-Burma region: Insights from cretaceous Nb-enriched and oceanic-island basalt-like mafic rocks. Geological Society of America Bulletin, 129(5-6), 698-714.

Liu, H., Li, Y., Wu, L., Huangfu, P., Zhang, M., 2018. Geochemistry of high-Nb basaltandesite in the Erguna Massif (NE China) and implications for the early Cretaceous back-arc extension. Geological Journal, 54(1), 291-307.

Manikyamba, C., Naqvi, S.M., Rao, D.V.S., Mohan, M.R., Khanna, T.C., Rao, T.G., Reddy, G.L.N., 2005. Boninites from the Neoarchean Gadwal greenstone belt, eastern Dharwar Craton, India: implications for Archean subduction processes. Earth and Planetary Science Letters, 230, 65-83.

Martin, H., Smithies, R.H., Rapp, R., Moyen, J.F., Champion, D., 2005. An overview of adakite, tonalite-trondhjemite-granodiorite (TTG), and sanukitoid: Relationships and some implications for crustal evolution. Lithos, 79(1-2), 1-24.

Mazhari, S.A., 2016. Petrogenesis of adakite and high-Nb basalt association in the SW of Sabzevar Zone, NE of Iran: evidence for slab melt-mantle interaction. Journal of African Earth Sciences, 116, 170-181.

McCulloch, M.T., Gamble, A.J., 1991. Geochemical and geodynamical constraints on subduction zone magmatism. Earth and Planetary Science Letters, 102, 358-374.

Mckenzie, D., O'Nions, R.K., 1991. Partial melt distributions from inversion of rare Earth element concentrations. Journal of Petrology, 32, 1021-1091.

Misra, S., 2006. Precambrian chronostratigraphic growth of Singhbhum-Orissa Craton, Eastern Indian Shield: an alternative model. Journal of the Geological Society of India, 67, 356-378.

Pandey, O.M., Mezger, K., Ranjan, S., Upadhyay, D., Villa, I.M., Nagler, F.M., Vollsteadt, H., 2019. Genesis of the Singhbhum Craton, eastern India; implications for Archean crust-mantle evolution of the Earth. Chemical Geology, 512, 85-106.

Paul, M., Ray, J., Manikyamba, C., Ganguly, C., Singh, M.R., Pachal, S., Sarkar, D., 2020. Mafic volcanic rocks of western Iron Ore Group, Singhbhum Craton, eastern India: Geochemical evidence for ocean-continent convergence. Geological Journal, 56(1), 102-129.

Pearce, J.A., 1982. Trace element characteristics of lavas from destructive plate boundaries. In: Thorpe, R.S. (ed.). Andesites. Wiley, Chichester, 525-548.

Pearce, J.A., Parkinson, I.J., 1993. Trace element models for mantle melting: application to volcanic arc petrogenesis. Geological Society of London Special Publication, 76, 373-403.

Pearce, J.A., Peate, D.W., 1995. Tectonic implications of the composition of volcanic arc magmas. Annual Review of Earth and Planetary Science, 23, 251-285.

Pearce, J.A., 2008. Geochemical fingerprinting of oceanic basalts with applications to ophiolite classification and the search for Archean oceanic crust. Lithos, 100, 14-48.

Peccerillo, A., Taylor, S.R., 1976. Geochemistry of Eocene calc-alkaline volcanic rocks from the Kastamonu area, northern Turkey. Contributions to Mineralogy and Petrology, 58, 130-143.

Percival, J.A., Stern, R.A., Rayner, N., 2003. Archean adakites from the Ashuanipi complex, eastern Superior Province, Canada: Geochemistry, geochronology, and tectonic significance. Contributions to Mineralogy and Petrology, 145, 265-280.

Perfit, M.R., Gust, D.A., Bence, A.E., Arculus, R.J., Taylor, S.R., 1980. Chemical characteristics of island-arc basalts: implications for mantle sources. Chemical Geology, 30(3), 227-256.

Petrone, C.M., Francalanci, L., Ferrari, L., Schaaf, P., Conticelli, S., 2006. The San Pedro-Cerro Grande Volcanic Complex (Nayarit, Mexico): inferences on volcanology and magma evolution. In: Siebe, C., Aguirre-Dı'az, G., Macı'as, J.L. (eds.). Neogene-Quaternary Continental Margin Volcanism: A Perspective from Mexico, 402. Geological Society of America, 65-68.

Petrone, C.M., Ferrari, L., 2008. Quaternary adakite-Nb-enriched basalt association in the western Trans-Mexican Volcanic Belt: is there any slab melt evidence? Contributions to Mineralogy and Petrology, 156(1), 73-86.

Polat, A., Kerrich, R., 2001. Magnesian andesites, Nb-enriched basalt-andesites, and adakites from late-Archean 2.7 Ga Wawa greenstone belts, Superior Province, Canada: implications for late Archean subduction zone petrogenetic processes. Contributions to Mineralogy and Petrology, 141(1), 36-52.

Polat, A., Hofmann, A.W., Rosing, M.T., 2002. Boninite-like volcanic rocks in the 3.7-3.8 Ga Isua greenstone belt, West Greenland: geochemical evidence for intra-oceanic subduction zone processes in the early Earth. Chemical Geology, 184(3), 231-254.

Rapp, R.P., Shimizu, N., Norman, M.D., Applegate, G.S., 1999. Reaction between slab derived melts and peridotite in the mantle wedge: experimental constraints at 3.8 GPa. Chemical Geology, 160, 335-356.

Ray, J., Das, S., Bhattacharyya, P., 2006. Malangtoli lava of the eastern Indian shield: some aspects of major-element geochemistry and tectonic affiliation. Indian Minerals, 60, 55-68

Rudnick, R., Gao, S., 2003. Composition of the continental crust. Treatise on Geochemistry, 3, 1-64.

Saha, A.K., 1994. Crustal Evolution of Singhbhum-North Orissa, Eastern India, Memoir 27. Geological Society of India, 341pp.

Said, N., Kerrich, R., 2009. Geochemistry of coexisting depleted and enriched Paringa Basalts, in the 2.7 Ga Kalgoorlie Terrane, Yilgarn Craton, Western Australia: Evidence for a heterogeneous mantle plume event. Precambrian Research, 174, 287-309.

Sajona, F.G., Maury, R.C., Bellon, H., Cotten, J., Defant, M.J., Pubellier, M., 1993. Initiation of subduction and the generation of slab melts in western and eastern Mindanao, Philippines. Geology, 21(11), 1007-1010.

Sajona, F.G., Maury, R.C., Bellon, H., Cotten, J., Defant, M., 1996. High field strength element enrichment of pliocene-pleistocene island arc basalts, Zamboanga Peninsula, Western Mindanao (Philippines). Journal of Petrology, 37(3), 693-726.

Sharma, R.S., 2009. Cratons and Fold Belts of India. Heidelberg, Springer Verlag, 324pp.

Shen, X.M., Zhang, H.X., Wang, Q., Ma, L., Yang, Y.H., 2014. Early Silurian (w440 Ma) adakitic, andesitic and Nbeenriched basaltic lavas in the southern Altay Range, Northern Xinjiang (western China): slab melting and implications for crustal growth in the Central Asian Orogenic Belt. Lithos, 206-207, 234-251.

Singh, M.R., Manikyamba, C., Ganguly, S., Ray, J., Santosh, M., Singh, T.D., Kumar, B.C., 2017. Paleoproterozoic arc basalt-boninite-high magnesian andesite-Nb enriched basalt association from the Malangtoli volcanic suite, Singhbhum Craton, eastern India: geochemical record for subduction initiation to arc maturation continuum. Journal of Asian Earth Sciences, 134, 191-206.

Smithies, R.H., Champion, D.C., van Kranendonk, M.K., Howard, H.M., Hickman, A.H., 2005. Modern-style subduction processes in the Mesoarchean: geochemical evidence from the 3.12 Ga Whundo intra-oceanic arc. Earth and Planetary Science Letters, 231, 221-237.

Song, X.Y., Zhou, M.F., Keays, R.R., Cao, Z.M., Sun, M., Qi, L., 2006. Geochemistry of the Emeishan flood basalts at Yangliuping, Sichuan, SW China: Implications for sulphide segregation. Contributions to Mineralogy and Petrology, 152, 53-74.

Sorbadere, F., Schiano, P., Métrich, N., Bertagnini, A., 2013. Smalle scale coexistence of islande-arc and enriched-MORB-type basalts in the central Vanuatu arc. Contributions to Mineralogy and Petrology, 166, 1305-1321.

Spandler, C., Pirard, C., 2013. Element recycling from subducting slabs to arc crust: a review. Lithos, 170, 208-223.

Sreenivas, B., Dey, S., Rao, Y.B., Kumar, T.V., Babu, E.V.S.S.K., Williams, I.S., 2019. A new cache of Eoarchaean detrital zircons from the Singhbhum craton, eastern India and constraints on early Earth geodynamics. Geoscience Frontiers, 10, 1359-1370.

Sun, S.S., Mc Donough, W.F., 1989. Chemical and isotopic systematics of oceanic basalts, implications for mantle composition and processes. In: Saunders, A.D., Norry, M.J., (eds.). Magmatism in the Ocean Basins. London, The Geological Society, 42 (Special Publication), U.K., Blackwell Scientific Publication, 313-345.

Thirlwall, M.F., Smith, T.E., Graham, A.M., Theodorou, N., Hollings, P., Davidson, J.P., Arculus, R.J., 1994. High field strength element anomalies in arc lavas: source or process? Journal of Petrology, 35, 819-838.

Tiepolo, M., Vannucci, R., Oberti, R., Foley, S., Bottazzi, P., Zanetti, A., 2000. Nb and Ta incorporation and fractionation in titanian pargasite and kaersutite: crystal-chemical constraints and implications for natural systems. Earth and Planetary Science Letters, 176, 185-201.

Ujike, O., Goodwin, A.M., Shibata, T., 2007. Geochemistry of Archean volcanic rocks from the Upper Keewatin assemblage (ca. 2.7 Ga), Lake of the Woods greenstone belt, Western Wabigoon subprovince, Superior Province, Canada. Island Arc, 16, 191-208.

Wang, K.L., Chung, S.L., O'Reilly, S.Y., Sun, S.S., Shinjo, R., Chen, C.H., 2004. Geochemical constraints for the genesis of post-collisional magmatism and the geodynamic evolution of the northern Taiwan region. Journal of Petrology, 45, 975-1011.

Wang, Q., Wyman, D.A., Zhao, Z.H., Xu, J.F., Bai, Z.H., Xiong, X.L., Dai, T.M., Li, C.F., Chu, Z.Y., 2007. Petrogenesis of Carboniferous adakites and Nb-enriched arc basalts in the Alataw area, northern Tianshan Range (western China): implications for Phanerozoic crustal growth in the Central Asia orogenic belt. Chemical Geology, 236(1), 42-64.

Wang, Q., Wyman, D.A., Xu, J.F., Wan, Y., Li, C.F., Zi, F., Qiu, H.N., Chu, Z.Y., Zhao, Z.H., Dong, Y.H., 2008. Triassic Nb-enriched basalts, magnesian andesites, and adakites of the Qiangtang terrane (Central Tibet): evidence for metasomatism by slab-derived melts in the mantle wedge. Contributions to Mineralogy and Petrology, 155(4), 473-490.

Wang, Z.L., Deru, X.U., Chuanjun, W.U., Wangwei, F.U., Li, W., Jun, W., 2013. Discovery of the late Paleozoic ocean island basalts (OIB) in Hainan Island and their geodynamic implications. Acta Petrologica Sinica, 29(3), 875-886.

Weaver, B.L., 1990. Geochemistry of highly-undersaturated ocean island basalt suites from the South Atlantic Ocean: Fernando de Noronha and Trindade Islands. Contributions to Mineralogy and Petrology, 105, 502-515.

Wood, D.A., 1980. The application of a Th-Hf-Ta diagram to problems of tectonomagmatic classification and to establishing the nature of crustal contamination of basaltic lavas of the British Tertiary volcanic province. Earth and Planetary Science Letters, 50, 11-30.

Wyman, D.A., Ayer, J.A., Devaney, J.R., 2000. Niobium-enriched basalts from the Wabigoon subprovince, Canada: Evidence for adakitic metasomatism above an Archean subduction zone. Earth and Planetary Science Letters, 179(1), 21-30.

Xia, L.Q., Xia, Z.C., Xu, X.Y., Li, X.M., Ma, Z.P., 2009. Do the Tianshan Carboniferous volcanic successions contain Nbeenriched arc basalts? Earth Science Frontiers, 16(6), 303-317.

Xu, J., Xia, X.-P., Lai, C.-K., Zhou, M., Ma, P., 2019. First Identification of Late Permian Nb□Enriched Basalts in Ailaoshan Region (SW Yunnan, China): Contribution from Emeishan Plume to Subduction. Geophysical Research Letters, 46, 2511-2523.

Zhang, H., Niu, H., Sato, H., Yu, X., Shan, Q., Zhang, B., Ito, J., Nagao, T. 2005. Late Palaeozoic adakites and Nb-enriched basalts from northern Xinjiang northwest China: evidence for the southward subduction of the Paleo-Asian Oceanic plate. Island Arc, 14, 55-68.

Zhang, A.M., Wang, Y.J., Fan, W.M., Zhang, Y., Yang, J., 2012. Earliest Neoproterozoic (ca. 1.0 Ga) arcebackearc basin nature along the northern Yunkai Domain of the Cathaysia Block: geochronological and geochemical evidence from the metabasite. Precambrian Research, 220-221, 217-233.

Zhang, H.R., Yang, T., Hou, Z., Bian, Y., 2016. Devonian Nbeenriched basalts and andesites of northecentral Tibet: evidence for the early subduction of the PaleoeTethyan oceanic crust beneath the North Qiangtang Block. Tectonophysics, 682, 96-107.

Manuscript received November 2021;
revision accepted July 2022;
published Online September 2022.

APPENDIX I

TABLE 1. Major and trace concentrations og BHVO-1 and JB-2 obtained from XRF and ICP-MS

	BHVO-1				JB-2			
wt%	A	B	SD	%RSD	A	B	SD	%RSD
SiO_2	49.70	49.94	0.17	0.35	53.68	53.20	0.34	0.63
Al_2O_3	13.59	13.80	0.15	1.11	14.94	14.67	0.19	1.28
Fe_2O_3	12.28	12.23	0.04	0.29	14.83	14.34	0.35	2.34
MnO	0.16	0.16	0.00	1.36	0.21	0.20	0.01	3.37
MgO	7.53	7.23	0.21	2.87	4.78	4.66	0.08	1.78
CaO	11.51	11.40	0.08	0.69	9.68	9.89	0.15	1.53
Na_2O	2.17	2.26	0.06	2.79	2.01	2.03	0.01	0.70
K_2O	0.55	0.52	0.02	3.64	0.45	0.42	0.02	4.71
TiO_2	2.79	2.71	0.05	1.93	1.36	1.19	0.12	8.84
P_2O_5	0.24	0.24	0.00	0.73	0.10	0.10	0.00	0.00
ppm								
Sc	32.069	31.8	0.597	1.834	54.331	54.4	0.585	1.074
V	321.197	317	7.652	2.367	578.664	578	6.4	1.103
Cr	293.498	289	5.757	1.972	27.423	27.4	0.419	1.522
Co	45.343	45	1.043	2.304	40.411	39.8	0.355	0.891
Ni	121.363	121	1.887	1.544	13.976	14.2	0.165	1.183
Cu	136.719	136	1.785	1.298	226.78	227	0.945	0.416
Zn	106.077	105	2.664	2.506	110.392	110	2.256	2.051
Ga	21.248	21	0.361	1.709	17.076	17	0.3	1.75
Rb	11.101	11	0.109	0.997	6.185	6.2	0.085	1.384
Sr	407.279	403	4.674	1.156	179.56	178	1.937	1.092
Y	27.844	27.6	0.384	1.39	25.005	24.9	0.187	0.751
Zr	179.998	179	2.107	1.172	51.84	51.4	0.458	0.894
Nb	19.218	19	0.174	0.917	0.778	0.8	0.07	8.961
Cs	0.136	0.13	0.006	4.639	0.894	0.9	0.026	2.852
Ba	138.785	139	2.387	1.686	211.014	208	2.602	1.252
La	15.903	15.8	0.259	1.605	2.348	2.37	0.031	1.335
Ce	39.016	39	0.68	1.712	6.848	6.77	0.059	0.872
Pr	5.732	5.7	0.134	2.303	0.971	0.96	0.017	1.783
Nd	25.203	25.2	0.583	2.254	6.768	6.7	0.065	0.961
Sm	6.171	6.2	0.19	3.001	2.288	2.25	0.036	1.577
Eu	2.029	2.06	0.056	2.675	0.895	0.86	0.017	1.907
Gd	6.468	6.4	0.253	3.817	3.431	3.28	0.125	3.815
Tb	0.956	0.96	0.032	3.199	0.623	0.62	0.017	2.694
Dy	5.186	5.2	0.17	3.156	3.653	3.66	0.053	1.462
Ho	0.974	0.99	0.025	2.469	0.795	0.81	0.008	0.994
Er	2.417	2.4	0.106	4.285	2.647	2.63	0.035	1.333
Tm	0.331	0.33	0.015	4.282	0.452	0.45	0.004	0.805
Yb	2.07	2.02	0.083	3.934	2.552	2.51	0.054	2.115
Lu	0.293	0.29	0.022	7.186	0.395	0.39	0.013	3.363
Hf	4.359	4.38	0.239	5.196	1.425	1.42	0.024	1.742
Ta	1.231	1.23	0.062	4.794	0.194	0.2	0.016	8.305
Pb	2.596	2.6	0.127	4.621	5.399	5.4	0.107	1.993
Th	1.081	1.08	0.014	1.276	0.317	0.33	0.018	5.394
U	0.418	0.42	0.012	2.689	0.157	0.16	0.006	3.466

A: present study average of six values; B: Reported values from Govindaraju (1994) and GEOREM (georem.mpch-mainz.gwdg.de)

APPENDIX II

TABLE 2. Major (wt.%) and trace element (ppm) data for the Khandadharpahar-kadakala-Thakuranipahar sections, Malangtoli, Singhbhum craton

	Khandadharpahar-kadakala													
wt.%	KK 1	KK 2	KK 3	KK 4	KK 5	KK 6	KK 7	KK 8	KK 9	KK 10	KK 11	KK 12	KK 13	KK 14
SiO_2	53.29	54.34	53.78	53.51	51.31	54.71	54.80	55.65	55.38	54.58	54.27	54.87	54.88	54.09
TiO_2	1.16	1.09	0.84	0.85	1.12	1.07	1.09	1.07	1.11	1.08	1.10	1.08	1.07	1.09
Al_2O_3	11.90	10.87	12.29	12.27	13.53	11.71	11.01	10.52	11.01	11.79	11.05	11.51	11.77	12.70
Fe_2O_3	15.37	14.01	11.79	11.23	14.83	12.70	12.86	12.53	13.07	12.77	13.38	13.45	13.19	12.71
MnO	0.18	0.16	0.15	0.15	0.18	0.14	0.15	0.14	0.15	0.15	0.15	0.16	0.16	0.14
MgO	6.39	6.15	7.82	8.24	6.09	5.99	6.10	5.97	6.27	6.21	6.19	6.29	6.28	6.06
CaO	7.56	6.91	8.38	9.19	7.05	7.96	7.62	7.75	7.37	7.16	7.44	6.91	6.74	7.06
K_2O	1.25	1.80	1.40	1.28	1.59	1.86	1.68	1.73	1.95	1.81	1.78	2.00	1.80	1.76
Na_2O	2.60	2.66	2.04	1.77	2.55	2.62	2.93	2.86	2.49	2.60	2.60	2.27	2.47	2.89
P_2O_5	0.13	0.12	0.09	0.11	0.13	0.12	0.12	0.12	0.12	0.12	0.13	0.12	0.12	0.12
LOI	1.52	1.36	1.75	2.25	1.78	0.99	1.55	1.16	2.20	1.72	1.24	1.46	1.58	1.34
Sum	101.35	99.47	100.33	100.85	100.16	99.87	99.91	99.51	101.12	99.99	99.33	100.12	100.06	99.96
ppm														
Cr	36	25	88	96	24	24	29	25	26	28	25	32	30	33
Co	37	39	35	39	38	37	40	37	41	39	40	39	37	38
Ni	30	63	44	47	38	35	40	33	33	34	33	40	33	34
Rb	40	36	25	29	32	38	38	35	25	38	35	42	37	39
Sr	184	177	175	163	303	193	221	183	219	180	189	182	183	201
Cs	0.17	0.18	0.13	0.19	0.32	0.23	0.17	0.21	0.11	0.20	0.16	0.21	0.15	0.14
Ba	317	256	198	190	202	281	276	260	197	269	253	324	257	275
Ti	6954	6535	5036	5096	6714	6415	6535	6415	6654	6475	6595	6475	6415	6535
Sc	18.80	19.14	18.88	26.37	18.39	18.61	22.51	18.53	18.42	18.89	19.14	20.14	17.91	21.08
V	147	149	143	161	182	148	154	144	160	149	149	143	147	148
Ta	1.83	1.43	1.31	1.31	1.84	1.84	1.88	1.81	1.84	1.94	2.19	1.83	1.80	1.86
Nb	10.89	8.42	7.51	8.05	10.83	10.92	11.21	10.79	10.88	11.07	10.92	11.03	10.62	11.07
Zr	62.2	64.1	44.6	59.1	76.9	62.5	66.0	61.6	60.7	65.0	62.5	64.0	61.1	63.2
Hf	1.69	1.76	1.22	1.16	1.58	1.71	1.76	1.69	1.65	1.78	1.73	1.75	1.68	1.72
Th	4.06	3.58	2.68	3.14	3.80	3.88	4.15	3.82	3.49	3.90	3.87	4.02	3.71	3.98
U	0.90	0.85	0.59	0.64	0.86	0.86	0.90	0.84	3.93	0.87	0.86	0.86	0.85	0.91
Y	25.20	26.21	18.44	22.71	26.10	26.39	29.72	25.79	26.85	26.63	26.32	28.95	26.24	29.33
La	20.10	19.10	13.39	15.73	20.17	20.32	21.84	19.45	20.18	20.06	20.17	20.93	20.10	21.38
Ce	42.64	41.89	28.88	32.29	42.56	43.25	45.28	41.55	43.10	42.44	42.95	42.48	42.59	44.13
Pr	3.78	3.75	2.59	2.95	3.79	3.88	4.24	3.78	3.86	3.82	3.86	4.05	3.84	4.11
Nd	20.10	19.39	13.73	15.31	19.56	19.92	21.82	19.38	20.18	19.88	19.84	21.25	19.82	21.16
Sm	4.43	4.34	2.97	3.36	4.23	4.39	4.76	4.27	4.44	4.41	4.42	4.66	4.34	4.57
Eu	1.05	1.16	0.85	1.06	1.43	1.17	1.25	1.08	1.27	1.21	1.17	1.30	1.23	1.21
Gd	5.34	5.31	3.68	4.21	5.47	5.66	6.02	5.34	5.56	5.46	5.47	5.82	5.59	5.85
Tb	0.79	0.80	0.57	0.63	0.81	0.85	0.90	0.79	0.84	0.84	0.84	0.90	0.82	0.90
Dy	4.00	3.89	2.96	3.40	4.08	4.16	4.47	4.04	4.14	4.15	4.17	4.51	4.09	4.41
Ho	0.84	0.84	0.62	0.72	0.84	0.86	0.93	0.83	0.85	0.86	0.85	0.91	0.85	0.91
Er	2.66	2.68	1.98	2.24	2.57	2.67	2.89	2.59	2.64	2.72	2.70	2.85	2.64	2.79
Tm	0.43	0.43	0.32	0.36	0.43	0.45	0.48	0.42	0.43	0.44	0.44	0.48	0.44	0.46
Yb	2.28	2.41	1.71	1.96	2.28	2.49	2.69	2.36	2.44	2.49	2.44	2.61	2.41	2.55
Lu	0.35	0.34	0.26	0.29	0.32	0.35	0.37	0.35	0.35	0.36	0.35	0.38	0.35	0.37
Tol REE	108.78	106.33	74.49	84.49	108.52	110.39	117.95	106.22	110.30	109.13	109.65	113.11	109.12	114.78
Cu	117.9	119.1	101.1	83.9	94.7	110.9	116.0	116.4	109.3	118.5	117.6	118.5	112.4	111.0
Pb	3.6	3.9	4.6	4.9	11.0	3.4	3.9	3.4	3.5	3.5	3.4	4.1	4.1	3.7
Zn	59	68	42	49	64	61	53	58	65	58	69	55	56	56
Ga	13.4	14.3	12.2	13.6	23.6	14.6	15.1	13.8	16.3	13.9	14.9	14.2	14.9	14.4
Nb/Ta	5.95	5.88	5.75	6.17	5.88	5.94	5.97	5.96	5.90	5.72	4.98	6.03	5.91	5.95
Th/Nb	0.37	0.42	0.36	0.39	0.35	0.36	0.37	0.35	0.32	0.35	0.35	0.36	0.35	0.36
Nb/U	12.06	9.94	12.75	12.54	12.60	12.65	12.46	12.82	2.77	12.67	12.65	12.88	12.44	12.15
(La/Yb)n	6.33	5.69	5.61	5.74	6.35	5.86	5.82	5.92	5.93	5.78	5.92	5.76	5.98	6.02
(La/Sm)n	2.83	2.75	2.82	2.92	2.98	2.89	2.86	2.85	2.84	2.84	2.85	2.81	2.89	2.92
(Gd/Yb)n	1.90	1.78	1.74	1.73	1.94	1.84	1.81	1.83	1.84	1.78	1.81	1.81	1.88	1.86
(Nb/Th)pm	0.32	0.28	0.33	0.31	0.34	0.34	0.32	0.34	0.37	0.34	0.34	0.33	0.34	0.33
(Nb/La)pm	0.53	0.43	0.55	0.50	0.53	0.53	0.51	0.55	0.53	0.54	0.53	0.52	0.52	0.51
Eu/Eu*	0.66	0.74	0.78	0.86	0.91	0.72	0.71	0.69	0.78	0.75	0.73	0.76	0.77	0.72
Nb/Nb*	0.43	0.36	0.45	0.39	0.42	0.43	0.40	0.44	0.43	0.44	0.43	0.40	0.42	0.40

	Khandadharpahar-kadakala				Thakuranipahar							
wt.%	KK 15	KK 16	KK17	KK 18	TK 1	TK 2	TK 3	TK4	TK5	TK 6	TK 7	TK8
SiO_2	55.05	54.60	54.64	54.88	53.11	47.27	55.10	51.21	49.37	52.13	47.88	48.01
TiO_2	1.06	1.07	1.07	1.14	0.88	1.08	1.02	1.05	1.12	1.43	1.55	1.66
Al_2O_3	11.80	12.65	12.06	11.01	12.49	11.37	10.77	10.83	11.72	10.16	10.19	10.05
Fe_2O_3	12.95	12.13	12.20	14.51	11.60	12.19	8.90	11.74	11.46	12.12	11.77	12.32
MnO	0.15	0.15	0.14	0.17	0.16	0.17	0.12	0.16	0.15	0.17	0.14	0.15
MgO	6.11	6.20	5.92	6.32	8.07	14.91	9.02	12.39	13.04	9.37	12.13	12.62
CaO	7.03	6.84	8.34	7.20	8.58	7.09	6.30	5.37	6.87	10.01	10.70	9.79
K_2O	1.81	1.58	1.53	1.80	1.59	2.94	2.78	1.94	0.73	0.73	1.65	1.03
Na_2O	2.51	2.91	2.96	2.08	2.14	2.72	2.91	3.25	3.66	2.46	1.91	2.98
P_2O_5	0.12	0.12	0.12	0.13	0.09	0.14	0.13	0.13	0.17	0.21	0.16	0.16
LOI	1.43	1.45	1.26	1.61	1.46	1.92	1.97	1.73	1.96	1.45	1.14	1.06
Sum	100.02	99.70	100.24	100.85	100.17	101.80	99.02	99.80	100.25	100.24	99.22	99.83
ppm												
Cr	27	29	26	26	92	59	66	58	58	34	32	34
Co	39	38	39	38	35	50	32	46	44	44	45	44
Ni	32	33	33	35	41	38	30	36	35	24	24	24
Rb	38	29	30	34	33	59	62	45	15	24	37	22
Sr	183	160	200	200	188	87	68	81	102	238	321	248
Cs	0.15	0.12	0.14	0.13	0.18	0.37	0.37	0.33	0.21	0.22	0.32	0.20
Ba	278	230	216	239	240	417	471	463	320	234	364	208
Ti	6355	6415	6415	6834	5276	6475	6115	6295	6714	8573	9292	9952
Sc	18.63	17.18	18.55	18.50	23.18	26.97	26.01	26.90	26.47	30.25	29.71	30.12
V	148	145	152	150	153	178	169	179	178	282	263	262
Ta	2.23	1.85	1.94	1.86	1.51	1.22	1.03	1.24	0.86	2.25	1.99	2.11
Nb	10.75	11.36	11.37	11.13	8.10	10.34	9.96	10.60	9.99	22.83	22.19	22.48
Zr	62.2	63.4	64.6	82.4	46.9	173.3	165.4	166.5	183.6	275.2	270.1	293.6
Hf	1.73	1.69	1.73	1.68	1.25	3.90	3.60	3.72	4.34	5.39	5.29	6.00
Th	3.87	3.82	4.06	4.00	3.03	4.05	3.87	4.14	4.12	4.60	4.65	4.80
U	0.85	0.87	0.91	0.89	0.65	0.72	0.68	0.72	0.85	0.66	0.70	0.71
Y	25.99	25.09	26.53	25.87	20.95	28.04	28.45	28.81	29.85	45.82	45.01	45.32
La	20.26	18.98	19.88	19.78	14.85	21.83	22.43	20.34	24.46	32.60	32.47	31.95
Ce	42.46	41.84	42.72	42.02	31.31	45.83	43.64	44.28	49.91	66.72	67.20	66.53
Pr	3.82	3.72	3.82	3.82	2.77	4.43	4.37	4.41	4.79	6.32	6.41	6.37
Nd	19.76	19.58	20.10	20.11	14.78	22.20	21.91	22.31	23.46	32.06	31.65	31.69
Sm	4.35	4.32	4.47	4.48	3.26	4.38	4.34	4.35	4.50	6.13	6.02	6.11
Eu	1.17	1.14	1.06	1.26	0.90	1.25	1.17	0.86	1.26	1.59	1.72	1.60
Gd	5.39	5.25	5.35	5.36	3.93	4.93	5.04	5.17	5.18	7.34	7.27	7.37
Tb	0.81	0.78	0.82	0.81	0.62	0.79	0.80	0.78	0.81	1.21	1.23	1.23
Dy	4.16	4.06	4.25	4.19	3.19	4.22	4.38	4.37	4.37	6.79	6.80	6.71
Ho	0.86	0.83	0.86	0.82	0.69	0.90	0.93	0.95	0.96	1.46	1.44	1.48
Er	2.68	2.61	2.75	2.71	2.16	2.95	2.97	2.95	3.13	4.76	4.76	4.82
Tm	0.44	0.41	0.43	0.43	0.35	0.49	0.50	0.50	0.51	0.77	0.78	0.79
Yb	2.38	2.25	2.40	2.33	1.92	2.54	2.61	2.62	2.78	4.28	4.20	4.36
Lu	0.35	0.34	0.36	0.36	0.29	0.41	0.40	0.40	0.44	0.63	0.65	0.66
Tol REE	108.88	106.10	109.26	108.47	81.01	117.16	115.48	114.29	126.56	172.68	172.61	171.66
Cu	122.3	119.4	115.0	112.3	82.9	86.0	131.5	74.5	73.7	103.8	106.5	106.6
Pb	3.4	4.1	3.6	4.6	3.3	6.9	5.2	7.2	7.6	7.3	7.6	3.6
Zn	66	56	60	65	46	112	58	119	115	125	126	93
Ga	14.4	13.8	15.3	17.0	14.1	18.3	14.8	12.5	17.6	18.3	18.8	17.5
Nb/Ta	4.83	6.14	5.86	5.97	5.35	8.46	9.68	8.58	11.62	10.16	11.13	10.63
Th/Nb	0.36	0.34	0.36	0.36	0.39	0.39	0.39	0.39	0.41	0.20	0.21	0.21
Nb/U	12.64	13.10	12.55	12.54	12.50	14.37	14.70	14.67	11.69	34.35	31.61	31.82
(La/Yb)n	6.09	6.06	5.93	6.09	5.54	6.15	6.17	5.57	6.31	5.46	5.55	5.25
(La/Sm)n	2.91	2.75	2.78	2.76	2.85	3.11	3.23	2.92	3.40	3.32	3.37	3.27
(Gd/Yb)n	1.83	1.89	1.80	1.86	1.65	1.57	1.56	1.60	1.51	1.39	1.40	1.37
(Nb/Th)pm	0.33	0.35	0.33	0.33	0.31	0.30	0.31	0.31	0.29	0.59	0.57	0.56
(Nb/La)pm	0.52	0.59	0.56	0.55	0.50	0.47	0.44	0.51	0.40	0.69	0.67	0.69
Eu/Eu*	0.74	0.73	0.66	0.79	0.77	0.82	0.76	0.55	0.79	0.72	0.79	0.73
Nb/Nb*	0.41	0.49	0.46	0.45	0.39	0.37	0.32	0.42	0.31	0.53	0.53	0.55